JOURNAL OF PROPULSION AND POWER
Vol. 10, No. 1, Jan.–Feb. 1994

Near-Wake Characteristics of Various V-Shaped Bluff Bodies

Jing-Tang Yang,* Go-Long Tsai,† and Wen-Bin Wang†
National Tsing Hua University, Hsinchu, Taiwan 30043, Republic of China

Mechanism of vortex shedding and turbulent flow features of the near-wake flow behind regular/irregular v-shaped bluff bodies are experimentally investigated at various airflow speeds between 10–60 m/s. With the aid of schlieren photography and a three-beam, two-component backward-scattering LDA system, the phenomena of vortex shedding and flow recirculation behind the flameholder are well illustrated. Results show Strouhal numbers, based on vortex shedding frequencies, being independent of gutter shape and within a range of 0.23–0.25. A similar flow structure of flow exists among near wake flows of v-gutters with different span angles. Increase of Reynolds number monotonically reduces the size of the recirculation zone. Variation in attack angle only slightly changes mean flow features, but enhances normalized Reynolds shear stresses in the near-wake.

Introduction

INTRODUCING a bluff body into the airstream is an effective way of holding the flame in ramjet combustors and thrust augmenters. Ample evidence has shown aerodynamic characteristics of the near-wake flow behind a v-gutter having crucial influence on flame structures and flameholding mechanisms. This type of flow, however, is associated with complicated phenomena such as separation and recirculation, mass entrainment through the shear layers, and vortex shedding. Many of these detailed mechanisms have not yet been well understood.

Extensive research[1–4] was conducted on ranges of fuel concentration, flow velocity, fuel air ratio, and blockage ratio with the flame stably sustained. Nicholson and Field[5] compared various experimental methodologies; they also used a high-speed camera for recording the wake flow patterns. Longwell[6] and William et al.[7] investigated effects of the mixing on oscillation of flow velocity and pressure. Rao and Lefebvre[8] and Stwalley and Lefebvre[9] measured effects of flameholder shape on limits of stabilization. Previous research primarily focused on overall performance of flame stabilization of the gutter and flame stability limits. Little research concentrated on aerodynamical aspect.

Vortex shedding process in shear layers supposedly has a close interaction with wake flow structures. Roshko[10] used a hot wire anemometer and a pitot tube in investigating the flow past a circular cylinder at a very high Reynolds number of 10^7. Strouhal number increased with Reynolds number when the Reynolds number was less than 3.5×10^6. Future research on recirculation zone was proposed. Mechanism of formation and shedding of vortices in wake region were studied by Gerrad.[11] He used wake width as the characteristic length, determining the dimensionless vortex shedding frequency. Unal and Rockwell[12] used a water channel in exploring the wake flow with Reynolds number less than 5000. Good quality photographs of wake flow pattern at a low Reynolds number were obtained, reporting Strouhal number as remaining at 0.2, while the Reynolds number was higher than 1000.

Fujii et al.[13,14] used a hot wire anemometer and a one-color LDA in studying the anisotropic turbulent flow structure of a wedge at low velocities, investigating the differences between reacting flows and cold flows. Taylor and Whitelaw[15] conducted a comprehensive review and used a one-color LDA for measuring flow behaviors of wake flows for plane baffles, disks, and cones at velocities of an order of 1 m/s. Effects of local geometries of disks and cones on wake flows were discussed extensively. Acoustical diagnostic method was adopted by Hedge et al.[16] for studying wake flow, finding aerodynamics to be a main controlling factor in flame stabilization for a coaxial dump combustor.

Previous research has indicated near-wake flow as being very sensitive to flow velocity and geometry of v-gutter. Most research, however, has been restricted to flows with low velocity and wake characteristics being visualized in a water tunnel at a relatively low Reynolds number. For improving physical understanding and providing data for various numerical analyses on wake flow of v-shaped bluff bodies, influence of angle of attack and span angle on turbulent flow features at high flow velocities from 10 up to 60 m/s are studied here.

Experimental Techniques

Test Rig

Experiments were conducted in an open-circuit wind tunnel, blown by a 100-hp Rootsblower with the speed controlled by a Hitach frequency inverter. The blower provided a maximum flow rate of 50 m^3/min with a maximum static pressure of 7000-mm H_2O. The dimension of the test section was 10 by 10 cm. Configurations and dimensions of two of the tested v-gutters have been shown in Fig. 1. Flow structures were qualitatively observed through a schlieren system and quantitatively measured through measurements of velocities, pressures, and vortex shedding frequencies.

Instrumentations

Velocity measurements were made by a three-beam, two-component backward-scattering laser-Doppler anemometer (LDA), which was connected with a computer-controlled traversing system for two-dimensional movement. The resolution of transverse system was 0.03 mm. The whole set was mounted on an optical bench, being placed on a mill table for major movement.

Laser beam being emitted from a 5-W argon-ion laser, with the main emission wavelengths of 514.5 and 488 nm, was split into two beams. One of these two beams passed through a Bragg cell to produce a 40-MHz frequency shift, then being split again, through a color-selected beam splitter, into two beams with wavelengths of 514.5 and 488 nm, separately. The resulting two beams, together with the other original beam, then passed through a beam translator, a beam expander, and a convergent lens of the focal length of 310 mm, finally being

Received Dec. 5, 1989; revision received Dec. 14, 1991; accepted for publication March 16, 1993.

*Professor, Department of Power Mechanical Engineering. Member AIAA.

†Graduate Student, Department of Power Mechanical Engineering.

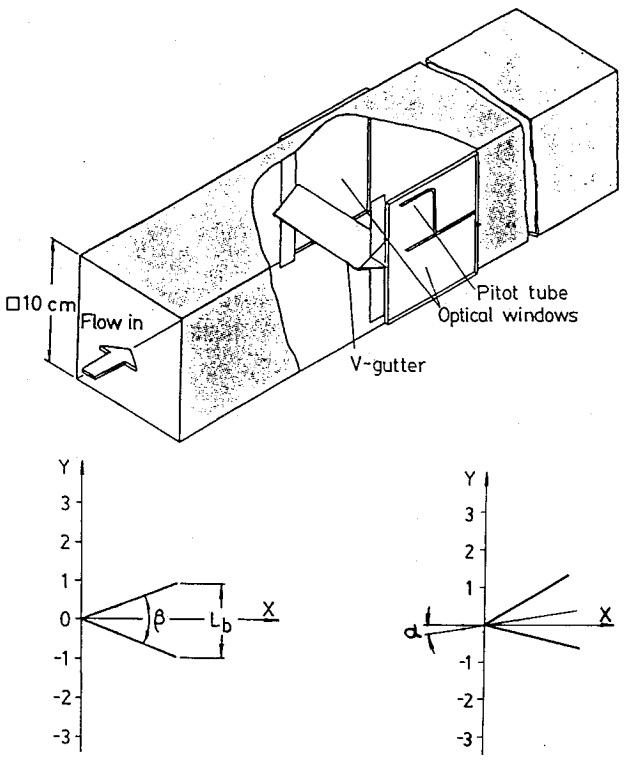

Fig. 1 Configurations and dimensions of tested v-gutters.

focused at the desired position. Two axes of optical probe volume were 0.128 and 0.135 mm, respectively. Backward-scattering Doppler signals were collected through two photomultipliers and processed by a coincidence filter and two counter processors. A beam waist adjustor was used in front of a whole optical system in order to obtain better signals. Seeding particles were generated from a Dantec seeding generator, heated, and then introduced into an airflow stream at a divergent section of the wind tunnel. Seeding particles were made of 25% glycerin resolvent with diameter in an order of 1 μm.

Flow was visualized through a schlieren system which included an Oriel 100-W mercury lamp, a 200-mm focal length condensing lens, a 0.2-mm pinhole, two 254-mm-diam (10-in.) concave mirrors, and a knife edge. For enhancing the contrast of schlieren images of the recirculation zone, two 50-μm-diam nichrome wires were separately attached to the edges of two wings of v-gutter. Wires were heated up electrically and made the neighboring fluid only 1°C higher than the environment. Images were recorded through a Sony F340 video camera with a time resolution of 0.03- and 1/4000-s shutter speed. A NAC high-speed camera was also used in assisting the observation of the history of vortices generation.

Measurements of vortex shedding frequencies were made by a 1.5-mm-o.d. L-shaped tube, with eight 0.1-mm holes drilled around the end of the tube. This device was capable of detecting transient signals of pressure up to 3 kHz. Detected data was then transmitted through a Kistler 7061 piezoelectric transducer, a charge amplifier, and a noise filter, and finally analyzed by a data translation 6100 waveform analyzer. Mean pressures were measured by traversing a tiny pitot tube every 2 mm across transversal direction, and every 5 mm along the axial direction in the recirculation zone.

Experimental Conditions

Two types of v-gutters 1) regular and 2) irregular types, were tested. Irregular v-gutters were nonsymmetric in respect to flow direction. Sketches of configuration, coordinate system, and dimensions of test section and v-gutter are shown in Fig. 1. Range of attack angle is from 0 to 15 deg. Span angle varies from 30 to 50 deg, corresponding to blockage ratios from 0.17 to 0.25. Range-of-flow velocity is 10–60 m/s, corresponding to Reynolds number, U_0L_b/ν, of 1.3×10^4 to 8×10^4, where L_b is the blockage width of tested v-gutters. Corresponding Mach number of highest velocity is 0.2. For obtaining better images of flow patterns, tests of flow visualization were conducted at a flow velocity of 1 m/s. Maximum turbulent intensity in front of v-gutter was less than 0.85%.

Data Accuracy

Two thousand forty eight measurements were typically made at each measure point. Corresponding maximum uncertainties were 3.2% of mean velocity and 4.9% of turbulent intensity for a 95% confidence level. Corresponding maximum uncertainty for Reynolds shear stress was 13%. Since definition of Reynolds shear stress was $-\overline{u'v'}$, a 5% error of rms of (u') and (v') would cause about a 13% uncertainty of Reynolds shear stress. Uncertainty of Reynolds shear stress was then much higher than those of mean velocity and turbulent intensity. Uncertainty of pressure data was estimated to be within 5%. Standard deviations of frequencies measured in the recirculation zone for each case were within 1 Hz.

Results and Discussion

Flow Visualization

In understanding geometrical effects on recirculation flows behind tested v-gutters and comparing results with the LDA measurements, a series of schlieren pictures for a regular v-gutter with a 30-deg span angle were taken every 0.03 s, as shown in Fig. 2. Pictures have clearly depicted formation, growth, and shedding phenomena for a typical cycle of vortices behind a regular v-gutter. A vortex, with the center being marked with "*", first appeared in the upper shear layer, as shown in photograph (1). After 0.03 s, a second vortex marked with "+" appeared a short distance behind the edge of the upper wing, being illustrated in the dark region of photograph (2). Meanwhile, the first vortex kept growing. Photograph (3) shows the first vortex beginning to shed from the upper shear layer upstream. The remaining photographs depict decay and oscillation of the first vortex in far-wake area and growth of the second vortex. Vortices formed on both sides merge at a fixed location near the rear stagnation point.

For a case of 50-deg span angle, Fig. 3a shows that initiation of vortex occurs and sheds away farther downstream. Figure 3b shows a case of 15-deg angle of attack with a span angle of 30 deg. Although the upper wing has a longer stable shear layer than the lower wing, positions where the upper and lower vortices are rolling up more closely resemble those in Fig. 2.

Vortex Shedding Frequency

Frequencies of the vortex shedding were also detected at 10 mm behind the gutter and 10 mm above the centerline. Frequencies did not vary as the measurement position was kept within the recirculation region. One typical result of a wake flow behind a regular v-gutter with a 30-deg span angle is shown in Fig. 4. Two major frequencies in the figure originate from two different sources: 1) pseudosound being generated from velocity fluctuation at a fixed position when vortices street passes; and 2) acoustic wave, being excited by the pressure difference between the freestream and recirculation zone during vortex formation, transmitting inside the test section with sonic speed. Frequency of pseudosound varied with flow velocity, evidently detected within a recirculation zone where the coherent vortex structure is still strong. The frequency of acoustic wave was verified at approximately 25 Hz for all cases.

Frequency of pseudosound was further converted into dimensionless Strouhal number, fL_b/U_0, where f denotes vortex shedding frequency, L_b is width of the blockage, and U_0 is the upstream velocity. Figure 5a shows when the span angle

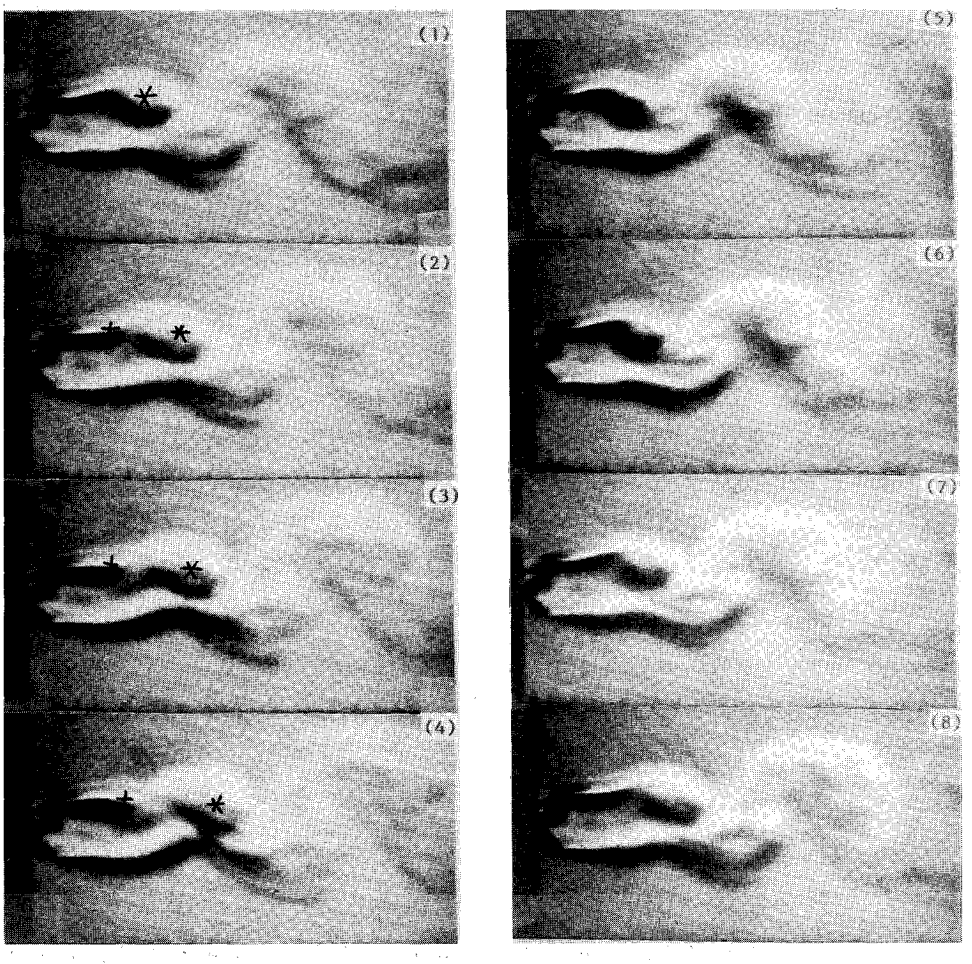

Fig. 2 Schlieren pictures of vortex shedding process of a regular v-gutter with a 30-deg span angle at U_0 = 1 m/s.

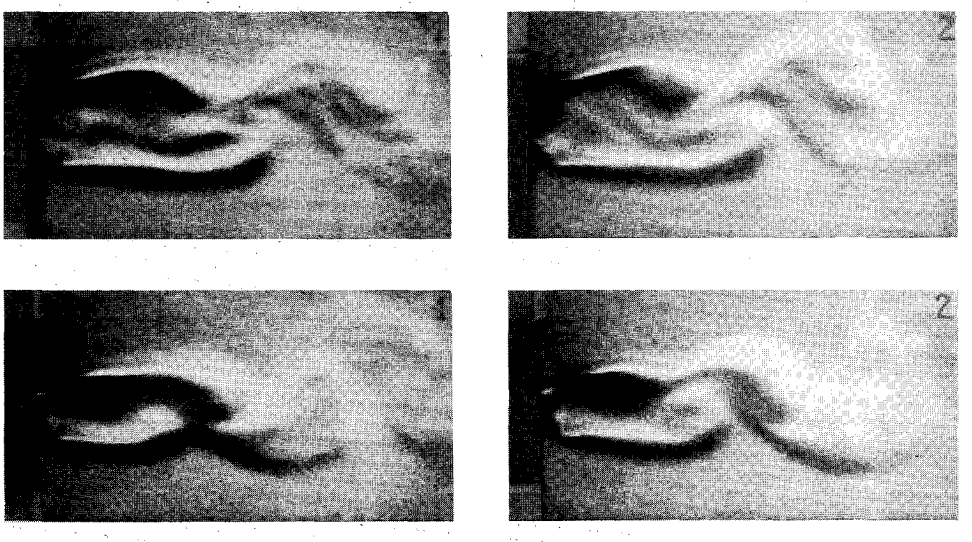

Fig. 3 Schlieren pictures taken at U_0 = 1 m/s for various configurations of v-gutter: a) regular v-gutter with a 50-deg span angle and b) irregular v-gutter with a 15-deg angle of attack and a 30-deg span angle.

varies from 30 to 45 deg, the Strouhal number remains near 0.24. When the Reynolds number was on an order of 10^4, based on the hydraulic diameter of the test section, the shedding frequency remained fairly constant.[12] Strouhal numbers of 50 deg were still between 0.25–0.27. Through LDA measurements, as shown in Fig. 6, the wall effect results in acceleration of outer flow and enhances the momentum difference between two sides of shear layers. Rate of vortex generation within the shear layer would then increase. Similarly, frequencies in 10- and 15-deg angles of attack, were slightly higher than those of a 0-deg angle of attack. Mean velocity distributions of gutters with 0-, 5-, and 15-deg angle of attack are illustrated in Fig. 7. Angle of attack generally has had a minor influence here on vortex shedding frequency, as indicated in Fig. 5b.

Flow Features

Typical flow pattern of recirculation flow is shown in Figs. 8a and 8b. Figure 8a depicts glycerine oil droplets flowing through a regular gutter of 30-deg span angle at U_0 = 60 m/s. A corresponding vector form of mean flowfield is shown in Fig. 8b. These two figures correspond very well. Figures

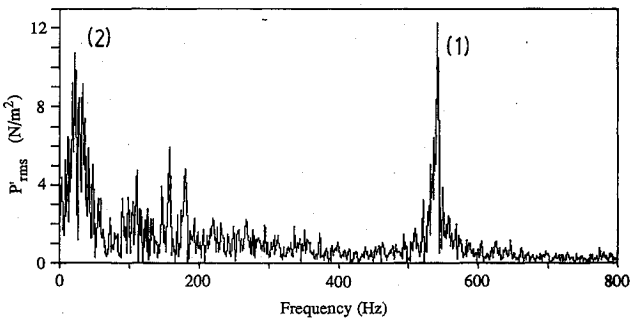

Fig. 4 Typical frequency spectrum of pressure fluctuation for a regular gutter with a 30-deg span angle at U_0 = 40 m/s.

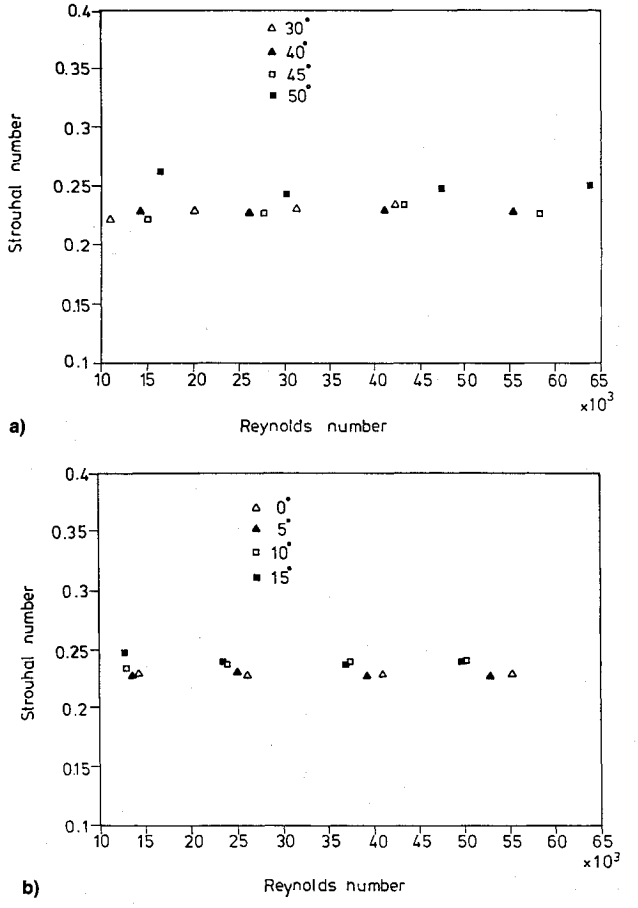

Fig. 5 Strouhal numbers vs Reynolds number for various: a) span angles and b) angles of attack.

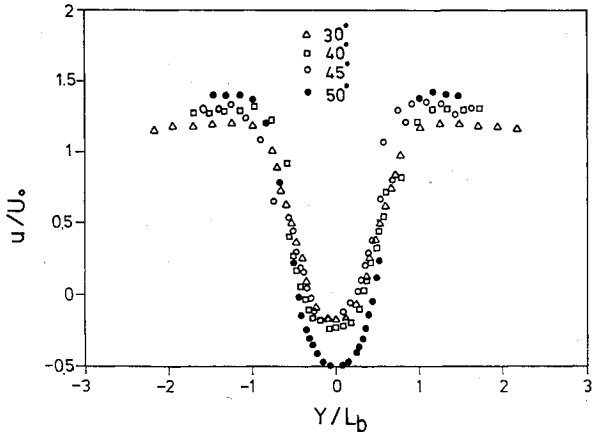

Fig. 6 Velocity profiles for various span angles at X/L_b = 1.75, U_0 = 20 m/s.

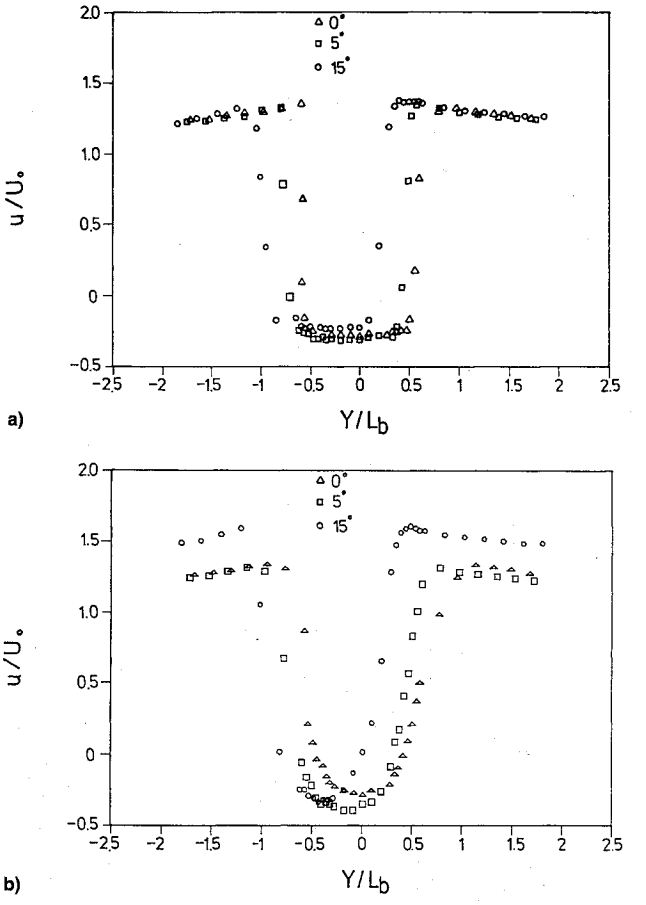

Fig. 7 Velocity profiles for various angles of attack at: a) X/L_b = 1.9, U_0 = 20 m/s and b) X/L_b = 2.3, U_0 = 20 m/s.

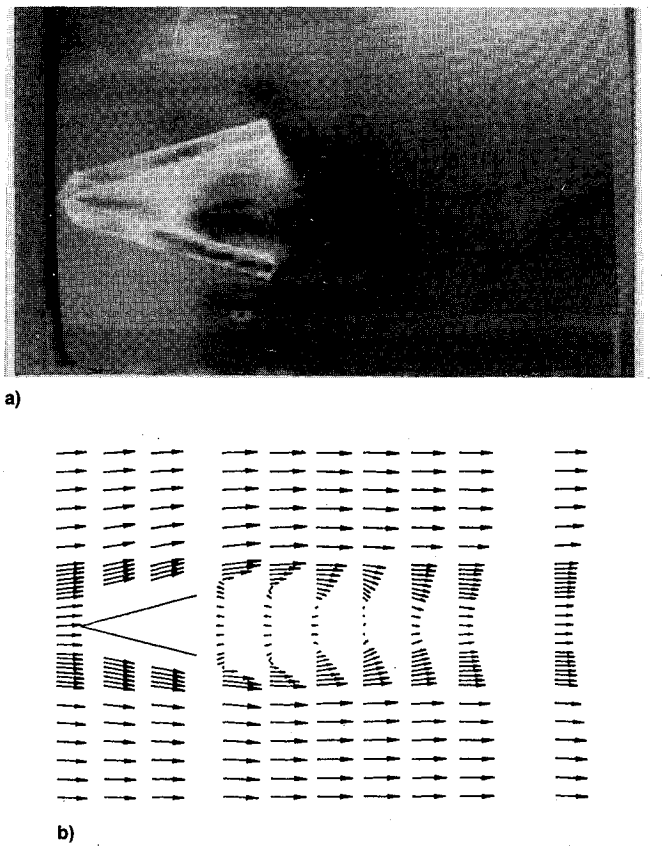

Fig. 8 a) Flow pattern of regular v-gutter with a 30-deg span angle at U_0 = 60 m/s and b) vector form of mean flowfield behind a regular v-gutter with a 30-deg span angle at U_0 = 60 m/s.

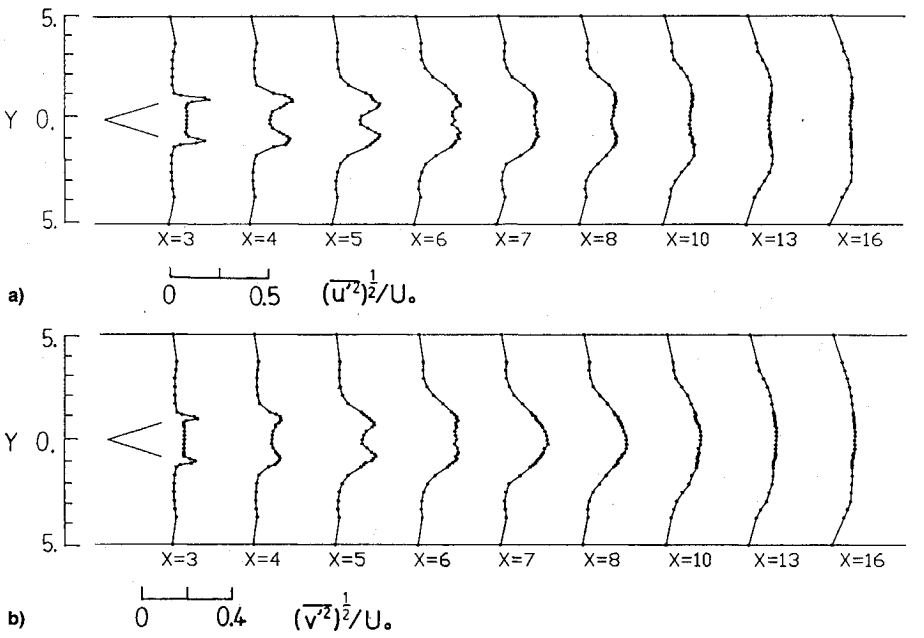

Fig. 9 Distributions of rms of both: a) axial velocity fluctuation at U_0 = 20 m/s and b) vertical velocity fluctuation at U_0 = 20 m/s for a regular v-gutter with a 30-deg span angle.

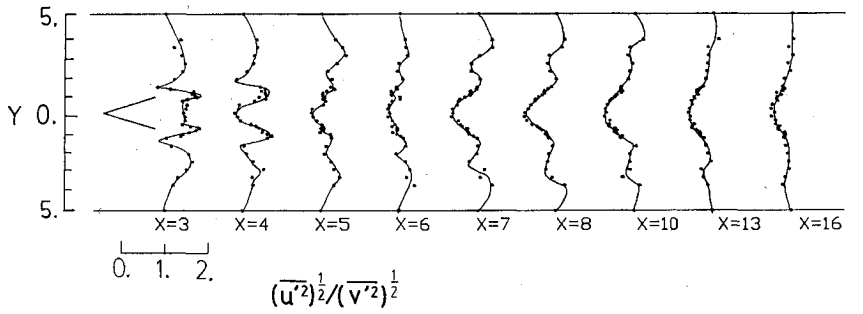

Fig. 10 Distribution of index of anisotropy at a flow behind a regular v-gutter with a 30-deg span angle at U_0 = 20 m/s.

9a and 9b show distributions of rms of axial velocity fluctuation $(\overline{u'^2})^{1/2}$, and transversal velocity fluctuation $(\overline{v'^2})^{1/2}$, both are similar. Peaks of fluctuation are at two shear layers, decaying along the sides of layers. Turbulent intensities increase as flow moves downstream and attain the maximum values near rear stagnation point.

Index of anisotropy in flow at several locations downstream of v-gutter can be expressed as a ratio of $(\overline{u'^2})^{1/2}$ to $(\overline{v'^2})^{1/2}$, as shown in Fig. 10. Since the streamline is significantly distorted by a large shear stress generated at the boundaries of shear layers, the maximum values of $(\overline{u'^2})^{1/2}$ and $(\overline{u'^2})^{1/2}/(\overline{v'^2})^{1/2}$ appear at inner edges of shear layers when x = 3 cm. Minimum values, meanwhile, appear at outer edges of shear layers. Entrainment of outer flow causes this, mixing with inner fluid. Two other peaks near the walls are due to an axial flow acceleration resulting from the narrowing of the path between walls and shear layers.

At a farther downstream position, i.e., x = 5 cm, vortices form and continuously grow larger. As a result, values of $(\overline{v'^2})^{1/2}$ then begin increasing, with widths of peaks in $(\overline{u'^2})^{1/2}/(\overline{v'^2})^{1/2}$ broadening gradually. Vortices generated on both sides of the v-gutter merge together, buffeting with each other at x = 6 cm. Behind the rear stagnation point, the distribution curve tends to flatten.

Vortices shedded from both upper and lower sides oscillate vertically, penetrating across the centerline of flow in turns between x = 7 cm and x = 8 cm. The effect enhances $(\overline{v'^2})^{1/2}$, resulting in very low values of $(\overline{u'^2})^{1/2}/(\overline{v'^2})^{1/2}$ along the centerline. Based on a distribution of $(\overline{u'^2})^{1/2}/(\overline{v'^2})^{1/2}$ at a downstream location of x = 16 cm, large and organized eddies can be assumed to have broken into small nonorganized eddies; therefore, the rate of turbulent energy dissipation and characteristics of isotropy then increase downstream.

The distribution of normalized Reynolds shear stress $(-\overline{u'v'}/U_0^2)$ corresponding to the test condition of Fig. 10 are asymmetric with respect to the centerline, as shown in Fig. 11. Peak normalized Reynolds shear stresses located at the outer edges of shear layers expand toward the walls; peak turbulent intensities, meanwhile, appear at the inner edges of shear layers, converging at the rear stagnation point. Maximum normalized Reynolds shear stress is also at a rear stagnation point of wake flow.

Typical two-dimensional static pressure distributions of wake flow are shown in Fig. 12. Reference pressure is chosen as static pressure at 10-cm upstream of the gutter. Recirculation zone is generally a low-pressure zone with a lowest value of C_p located at the "eye" of recirculation. Steep pressure gradients exist both in shear layers and near the rear stagnation point.

Effect of Gutter Configuration

In investigating the effect of angle of attack, a group of v-gutters with various angles of attack are tested. Mean velocity distributions under various angles of attack are shown in Fig. 7. Static pressure distributions of wake in a gutter with a 15-deg angle of attack and a 30-deg span angle are shown in Fig. 13. The value of C_p at the eye of the recirculation zone is 0.95, while a regular gutter being −1.05. Corresponding distribution of normalized Reynolds shear stress is shown in Fig. 14. Existence of angle of attack may shift the recirculation zone along a certain vertical distance and slightly change the size of the recirculation zone, as from the comparison among

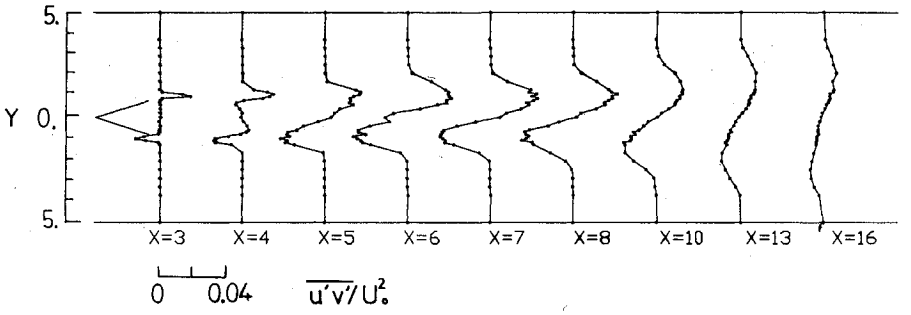

Fig. 11 Distributions of normalized Reynolds shear stress at U_0 = 20 m/s for a regular v-gutter with a 30-deg span angle.

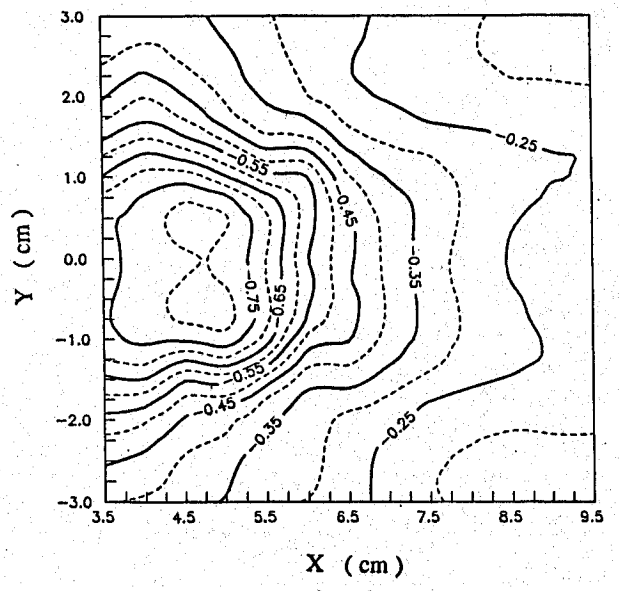

Fig. 12 Static pressure distributions of flow behind a regular v-gutter with a 30-deg span angle at U_0 = 20 m/s.

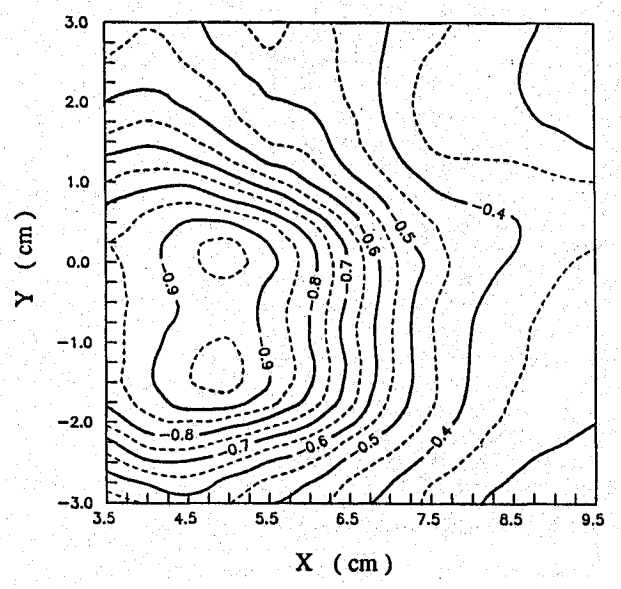

Fig. 13 Static pressure distributions of flow behind an irregular v-gutter with a 30-deg span angle and a 10-deg angle of attack at U_0 = 20 m/s.

Figs. 12, 13, and 7. In contrast to the symmetrical structure in Fig. 12, Reynolds stress between upper and lower wings are, however, quite different. Maximum Reynolds shear stress is 0.112, while the corresponding value for regular gutter is 0.062.

Effect of span angle of v-gutter on the size of the recirculation zone is depicted in Fig. 15. The rear stagnation point

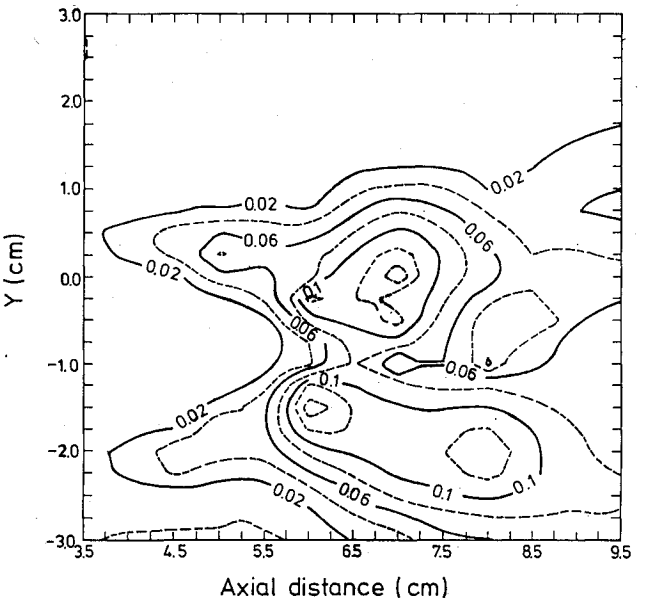

Fig. 14 Distributions of normalized Reynolds shear stress of flow behind an irregular v-gutter with a 30-deg span angle and a 10-deg angle of attack at U_0 = 20 m/s.

is taken as the location where reverse flow velocity is zero. Length of recirculation zone Xr is defined as the axial distance between rear stagnation point and origin. The larger the span angle, the longer the recirculation length. Dimensionless recirculation length Xr/L_b still stays constant at 3.5. Some sort of similarity in flow structure exists inside the recirculation zone. Rao and Lefebvre[8] performed similar measurements for the size of the recirculation zone behind a wedge, choosing the rear edge of a flameholder as the reference point. Their results did not show a unified trend. Exclusion of the influence in the boundary layer forming along the solid surface of the gutter in their choice might have been the crucial factor.

Taylor and Whitelaw[15] showed reverse mass flow rate being inversely proportional to the pressure of the eye in the recirculation zone. Their investigation showed values of C_p being -0.8, -1.05, and -1.3, respectively, corresponding to a span angle of 30, 40, and 50 deg when flow velocity was 20 m/s. Velocity distributions in Fig. 6 confirms that gutter with a 50-deg span angle causes the highest reverse flow rate as compared with other cases.

Maximum Reynolds shear stresses are 0.041, 0.062, 0.079, and 0.115, respectively, corresponding to span angles of 30, 40, 45, and 50 deg. The normalized location of maximum normalized Reynolds shear stress also shortens when the span angle is enlarged.

Effect of Reynolds Number

The length of the recirculation zone in a flowfield at 20 m/s is much longer than that of 60 m/s. The effect of Reynolds number on the length of the recirculation zone can be con-

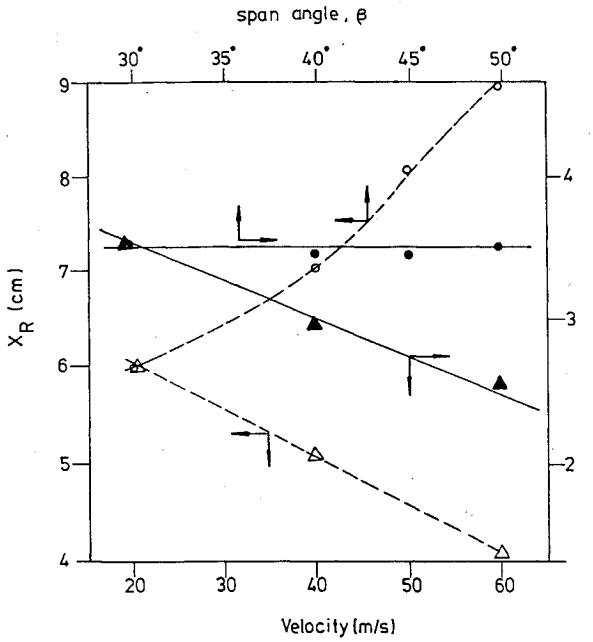

Fig. 15 Effects of span angle and velocity on length of recirculation zone.

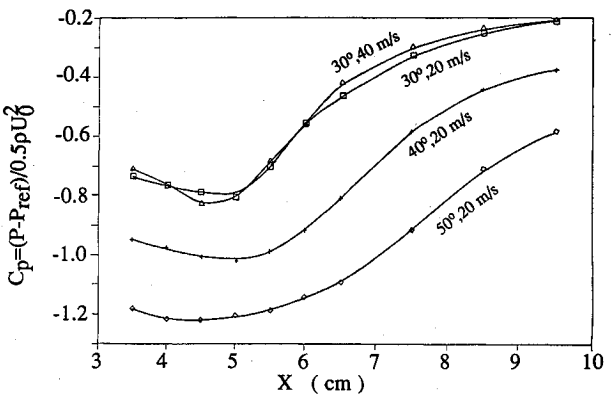

Fig. 16 Distributions of static pressure coefficient along centerline at various span angles and velocities.

cluded from Fig. 15. Since axial velocity near shear layers are proportional to momentum transferred from the outer stream, the length of recirculation zone is inversely proportional to flow velocity. However, adverse pressure gradient will curb the size of the recirculation zone. Figure 16 reveals adverse pressure gradient being proportional to velocity square. As flow velocity increases from 20 to 60 m/s, dimensionless recirculation length Xr/L_b is then monotonically reduced from 8 to 6. Increase of flow velocity may also push the eye of the recirculation zone upstream, although the C_p value does not significantly vary.

Conclusions

Features of near-wake flow behind various v-gutters have been clearly visualized and quantitatively measured in a range of airflow speed from 10 to 60 m/s. Based on the data presented, the following conclusions are made:

1) Static pressure fluctuation of near-wake originated from both components of pseudosound wave and acoustic wave. The frequency of pseudosound wave is greatly influenced by blockage ratio. Strouhal numbers are close to 0.23 when the span angle of regular v-gutter is changed from 30 to 45 deg. When blockage ratio is larger than 0.23, however, wall effect will have to be taken into account. Wall effect leads to acceleration of outer flow and enhances the momentum difference across shear layers.

2) Length of recirculation zone linearly decreases with an increase of Reynolds number. Similarity is also found among wake flows behind gutters with different span angles. Normalized length of recirculation zone stays constant as span angle varies from 30 to 50 deg.

3) Variation of angle of attack may shift recirculation zone to a certain vertical distance, but only slightly change the size of the recirculation zone. Maximum Reynolds shear stress, however, is distorted and enhanced at a higher angle of attack.

Acknowledgments

This work was partially supported by the National Science Council of the Republic of China, under Contract NSC77-0401-E007-15. The authors wish to thank Hsin-Min Law for his assistance in setting up the experiments.

References

[1]Chang, P. K., *Separation of Flow*, Pergamon, New York, 1970, Chap. 8.

[2]Zukoski, E. E., "Afterburners," *The Aerothermodynamics of Aircraft Gas Turbine Engines*, edited by G. C. Oates, AIAA Education Series, AIAA, New York, 1978, Chap. 21.

[3]Lefebvre, A. H., *Gas Turbine Combustion*, Hemisphere, New York, 1983, Chap. 6.

[4]Kundu, K. M., Banerjee, D., and Bhaduri, D., "On Flame Stabilization by Bluff-Bodies," *Journal of Engineering of Power*, Vol. 102, Jan. 1980, pp. 209–214.

[5]Nicholson, H. M., and Field, J. P., "Some Experimental Techniques for the Investigation of the Mechanism of Bluff Bodies," *Third Symposium (International) on Combustion, Flame, and Explosion Phenomena*, Williams and Wilkins, Baltimore, MD, 1949, pp. 44–68.

[6]Longwell, J. P., "Flame Stabilization by Bluff Bodies and Turbulent Flames in Ducts," *4th Symposium (International) on Combustion*, The Combustion Institute, Pittsburgh, PA, 1952, pp. 90–97.

[7]Williams, G. C., Hottel, H. C., and Scurlock, A. C., "Flame Stabilization and Propagation in High Velocity Gas Stream," *3rd Symposium (International) on Combustion, Flame, and Explosion Phenomena*, Williams and Wilkins, Baltimore, MD, 1949, pp. 21–40.

[8]Rao, K. V. L., and Lefebvre, A. H., "Flame Blowoff Studies Using Large-Scale Flameholders," *Journal of Engineering for Gas Turbines and Power*, Vol. 104, Oct. 1982, pp. 853–857.

[9]Stwalley, R. M., and Lefebvre, A. H., "Flame Stabilization Using Large Flameholders of Irregular Shape," *Journal of Propulsion and Power*, Vol. 4, No. 1, 1988, pp. 4–13.

[10]Roshko, A., "Experiments on the Flow Past a Circular Cylinder at Very High Reynolds Number," *Journal of Fluid Mechanics*, Vol. 10, 1961, pp. 345–356.

[11]Gerrad, J. H., "The Mechanics of the Formation Region of Vortices Behind Bluff Bodies," *Journal of Fluid Mechanics*, Vol. 25, 1966, pp. 401–413.

[12]Unal, M. F., and Rockwell, D., "On Vortex Formation from a Cylinder. Part 1. The Initial Instability," *Journal of Fluid Mechanics*, Vol. 190, 1988, pp. 491–512.

[13]Fujii, S., Gomi, M., and Eguchi, K., "Cold Flow Tests of a Bluff-Body Flame Stabilizer," *Journal of Fluids Engineering*, Vol. 100, Sept. 1978, pp. 323–332.

[14]Fujii, S., and Eguchi, K., "A Comparison of Cold and Reacting Flows Around a Bluff Body Flame Stabilizer," *Journal of Fluids Engineering*, Vol. 103, No. 2, 1981, pp. 328–334.

[15]Taylor, A. M. K. P., and Whitelaw, J. H., "Velocity Characteristics in the Turbulent Near Wakes of Confined Axisymmetric Bluff Bodies," *Journal of Fluid Mechanics*, Vol. 139, 1984, pp. 391–410.

[16]Hedge, U. G., Reuther, D., Zinn, B. T., and Daniel, B. R., "Fluid Mechanically Coupled Combustion-Instabilities in Ramjet Combustors," AIAA Paper 87-0216, June 1987.